AAS 17-711

SOLAR SAILING AT THE L4/L5 LIBRATION POINTS

Ariadna Farrés[*], Narcís Miguel[†]

In this paper we focus on the dynamics of a solar sail in the vicinity of the Lagrangian points L4/L5. These points are linearly stable and so are the families of quasi-periodic orbits around them. Moreover, there is a region of effective stability around them, where the trajectory of a satellite will remain there for more than 1000 years. We will describe these regions and see how they are affected by the solar radiation pressure. A good understanding of these regions and of how to reach them would enable a novel space weather mission

INTRODUCTION

Solar sails are a low-thrust propulsion system that takes advantage of the Solar Radiation Pressure (SRP) to accelerate a small probe by means of a highly reflecting surface. This technology enables new and challenging mission concepts such as the SunJammer mission, GeoSail, PoleSitter or even low-cost multi-rendezvous NEO mission. Up to the date there have been three successful solar sail demonstration missions: IKAROS by JAXA (May 2010), NanoSail-D by NASA (December 2010) and LightSail-1 by The Planetary Society (June 2016). In the next two years two more demonstration missions have been planned, LightSail-2 and NEO-Scout, which will prove the capabilities of solar sails.

The Earth - Sun Restricted Three Body Problem (RTBP) is a well known reference model in astrodynamics and has been extensively studied in the past. It is well known that the system has five equilibrium points. Three of them (L_1, L_2 and L_3) lie on the line joining the two primaries and are linearly unstable; the other two (L_4 and L_5) lie on the ecliptic plane forming an equilateral triangle with the two primaries and are linearly stable. Due to their location close to the Earth and their dynamical properties, periodic orbits around L_1 and L_2 are used as reference orbits for several mission applications such as SOHO, GAIA, Hershel-Plank, James Webb Space Telescope, among others. On the other hand, despite the orbits around L_4 and L_5 are stable and no station keeping is required, these equilibria have been forgotten for mission applications as they are hard to reach. Recent studies[1,2] have shown that using a solar sail enables to reach the vicinity of L_4 and L_5 in a reasonable time without increasing the total cost.

An interesting mission concept taking advantage of the L_4/L_5 regions would be to place simultaneously two satellites, one at L_4 and the other at L_5, monitoring the Sun's activity from two different points of view. This would allow to track the evolution of Sun spots and geomagnetic storms. The final goal of this project is to study in more detail the feasibility of this mission concept using solar sails or low-thrust propulsion systems. However, in this paper we will focus on describing the

[*]Dr. Visiting Researcher, NASA Goddard Space Flight Center, Greenbelt, Maryland
[†]Dr. Departament de Matemàtiques i Informàtica, Universitat de Barcelona, Barcelona

dynamics of a solar sail in the vicinity of L_4 and L_5 and explore the capabilities to remain in these regions and navigate around them.

As a model we consider the classical RTBP including the SRP due to the solar sail. The sail acceleration will depend on 3 parameters: the sail lightness number β (accounting for the sail efficiency), and two angles α, δ (accounting for the sail orientation). We will show how the different sail parameters affect the non-linear dynamics of the system around L_4 and L_5.

First we will describe how the solar sail acceleration affects the equilibrium points of the system and the dynamics around them. We will see how, for a fixed value of β, changes on the sail orientation (α, δ) "artificially" displace the location of these points. The same happens for the families of periodic orbits around them.[3] Second, we will focus on the stability regions around L_4/L_5. These are two regions in the vicinity of L_4/L_5 where the trajectory of a probe does not escape for more than 1000 years.[4] In order to compute these regions we have performed a brute force exploration by considering a set of initial conditions close to L_4 and L_5, integrating them for more than 1000 years and keeping those initial conditions that remain within the vicinity of L_4 and L_5, respectively. We will show how the extra effect of the solar sail affects these regions as we change the sail orientation. We will also classify the types of motion inside these regions. As we have already mentioned the goal of this study is to have a good understanding of the dynamics around L_4 and L_5 with a solar sail in order to provide target orbits for future space weather missions.

This paper is structured as follows: the first section is devoted to the description of the dynamical model that we have used (RTBPS) and its main parameters. We also summarize some of the most relevant properties of the system. The second section is devoted to the description of the families of equilibrium points and their stability as a function of the sail parameters. Section three focuses on the practical stability regions. There we outline how to compute these regions and discuss the results one obtains for different sail parameters. We end up with some conclusions and future work.

EQUATIONS OF MOTION

To describe the motion of a solar sail in the Earth - Sun system we consider as a model the Circular Restricted Three Body Problem (RTBP) adding the Solar Radiation Pressure (SRP) due to the solar sail (RTBPS). We assume that the Earth and Sun are both point masses moving around their common center of mass in a circular way due to their mutual gravitational attraction. The solar sail, on the other hand, is assumed to be a mass-less particle that does not affect the motion of the two primaries, but is affected by their gravitational attraction as well as by the SRP.

We use normalized units of mass, distance and time, so that the total mass of the system is 1, the Earth - Sun distance is 1 and the period of its orbit is 2π. In these units the universal gravitational constant is $G = 1$, the Earth's mass is $\mu = 3.0034806 \times 10^{-6}$, and $1 - \mu$ is the mass of the Sun. We consider a synodical reference system, where the origin is at the center of mass of the Earth - Sun system and both Earth and Sun are fixed on the x-axis (with its positive side pointing towards the Sun). The z-axis is perpendicular to the ecliptic plane and the y-axis completes an orthogonal positive oriented reference system[5] (Figure 1 left).

With these assumptions, the equations of motion in the synodical reference frame are:

$$\begin{aligned} \ddot{x} - 2\dot{y} &= x + (1-\mu)\frac{x-\mu}{r_{ps}^3} + \mu\frac{x-\mu+1}{r_{pe}^3} + a_x, \\ \ddot{y} + 2\dot{x} &= y + \left(\frac{1-\mu}{r_{ps}^3} + \frac{\mu}{r_{pe}^3}\right) y + a_y, \\ \ddot{z} &= \left(\frac{1-\mu}{r_{ps}^3} + \frac{\mu}{r_{pe}^3}\right) z + a_z, \end{aligned} \tag{1}$$

where $\mathbf{a} = (a_x, a_y, a_z)$ is the acceleration due to the solar sail, and $r_{ps} = \sqrt{(x-\mu)^2 + y^2 + z^2}$, $r_{pe} = \sqrt{(x-\mu+1)^2 + y^2 + z^2}$ are the Sun-sail and Earth-sail distances, respectively.

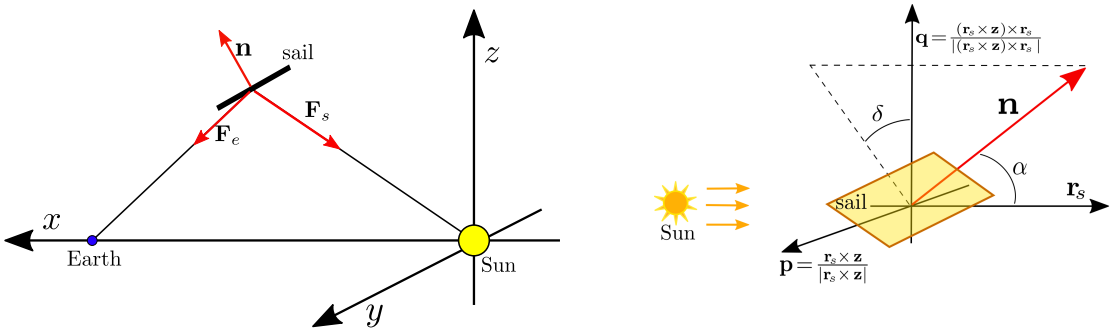

Figure 1. Left: Schematic representation of the RTBPS model. Right: Schematic representation of the reference frame used to define the sail orientation α, δ.

Solar Sail acceleration

The acceleration due to the solar sail depends on three parameters: two angles α, δ that define the solar sail's orientation, and the sail lightness number β that represents the sail's efficiency. In this paper we assume the solar sail to be flat and perfectly reflecting, so the acceleration due to SRP is in the normal direction to the surface of the solar sail ($\mathbf{n}$). For a more realistic approach one must also include the effect due to absorption and specluar reflection on the sail's surface. These two effects essentially affect the efficiency of the sail and slightly change the direction in which the sail's acceleration acts.[6] Hence, for a preliminary study, assuming a perfectly reflecting solar sail is good enough.

The sail orientation is given by the normal direction to the surface of the sail ($\mathbf{n}$) and is parameterised by two angles α and δ that measure the displacement between $\mathbf{n}$ and the Sun-sail direction $\mathbf{r_s} = (x-\mu, y, z)/r_{ps}$. Following McInnes,[7] we consider the orthonormal reference frame, $\{\mathbf{r}_s, \mathbf{p}, \mathbf{q}\}$, centered at the sailcraft center of mass, with $\mathbf{p} = \frac{\mathbf{r}_s \times \mathbf{z}}{|\mathbf{r}_s \times \mathbf{z}|}$ and $\mathbf{q} = \frac{(\mathbf{r}_s \times \mathbf{z}) \times \mathbf{r}_s}{|(\mathbf{r}_s \times \mathbf{z}) \times \mathbf{r}_s|}$, and define $\mathbf{n} = \cos\alpha\, \mathbf{r}_s + \sin\alpha\cos\delta\, \mathbf{p} + \sin\alpha\sin\delta\, \mathbf{q}$, where α corresponds to the pitch angle (angle between $\mathbf{n}$ and $\mathbf{r_s}$) and δ is the clock angle (angle between $\mathbf{q}$ and the projection of $\mathbf{n}$ in a plane orthogonal to $\mathbf{r}_s$). Figure 1 right shows a schematic representation of the definition of the two sail angles. Notice that $\mathbf{n}$ cannot point towards the Sun, hence $\langle \mathbf{n}, \mathbf{r_s} \rangle = \cos\alpha \geq 0$. This implies that $\alpha \in [-\pi/2, \pi/2]$ and $\delta \in [0, \pi]$.

Following the definitions given above, the explicit expressions for the solar sail normal direction, $\mathbf{n} = (n_x, n_y, n_z)$, are given by:

$$\begin{aligned} n_x &= \frac{x-\mu}{r_{ps}}\cos\alpha - \frac{(x-\mu)z}{r_2 r_{ps}}\sin\alpha\cos\delta + \frac{y}{r_2}\sin\alpha\sin\delta, \\ n_y &= \frac{y}{r_{ps}}\cos\alpha - \frac{yz}{r_2 r_{ps}}\sin\alpha\cos\delta - \frac{x-\mu}{r_2}\sin\alpha\sin\delta, \\ n_z &= \frac{z}{r_{ps}}\cos\alpha + \frac{r_2}{r_{ps}}\sin\alpha\cos\delta, \end{aligned} \tag{2}$$

where $r_2 = \sqrt{(x-\mu)^2 + y^2}$.

The force exerted by the photons that are reflected on the surface of the sail on a perfectly reflecting solar sail of area A is given by $\mathbf{F_r} = 2PA\langle \mathbf{n}, \mathbf{r_s}\rangle^2 \mathbf{n}$, where $P = P_0(R_0/R)^2$ is the SRP at a distance R from the Sun (being $P_0 = 4.563$ N/m^2 the SRP at $R_0 = 1$ AU). Recall that $\mathbf{r_s}$ is the Sun-sail direction and $\mathbf{n}$ is the normal direction to the surface of the sail (both unit vectors). Notice that the SRP acceleration is proportional to the inverse square of the distance to the Sun. So it is commonly rewritten as a correction of the Sun's gravitational attraction:

$$\mathbf{a} = \beta\frac{(1-\mu)}{r_{ps}^2}\langle \mathbf{r_s}, \mathbf{n}\rangle^2 \mathbf{n}, \tag{3}$$

where β corresponds to the sail lightness number, that accounts for the sail's efficiency. One can also interpret β as the ratio between the Sun's gravitational attraction and the solar sail acceleration. It is easy to see that,[8]

$$\beta = \sigma^*/\sigma, \qquad \sigma^* = \frac{2P_0R_0^2}{Gm_s} = 1.53 \text{ g/m}^2, \tag{4}$$

where $\sigma = m/A$ is the solar sail's mass-to-area ratio. Another way to describe the sail efficiency is by means of the characteristic acceleration (a_0), the acceleration experienced by the sailcraft at 1 AU when face-on to the Sun. The characteristic acceleration and the sail lightness number can easily be related by: $a_0 = \beta G m_{sun}/R_0^2$.

Table 1 shows, for different values of the sail lightness number (β), the corresponding area-to-mass ratio (σ), the characteristic acceleration (a_0) and the required solar sail size for 10 kg of total sailcraft mass. For instance, a sail lightness number $\beta = 0.03$ would provide a characteristic acceleration of 0.179804 mm/s^2, and requires a 14×14 m^2 solar sail for a 10 kg spacecraft.

Table 1. Relation between the sail lightness number β and: the satellite's area-to-mass ratio (σ), the characteristic acceleration (a_0), and the sail area required for a satellite with 10 kg of total mass.

β	σ (g/m^2)	a_0 (mm/s^2)	Area (m^2)
0.01	153.0	0.059935	$\approx 8 \times 8$
0.02	76.5	0.119869	$\approx 12 \times 12$
0.03	51.0	0.179804	$\approx 14 \times 14$
0.04	38.25	0.239739	$\approx 16 \times 16$
0.05	30.6	0.359608	$\approx 20 \times 20$

Properties of the RTBPS

From a mathematical perspective the Earth-Sun-sail RTBPS is as a perturbation of the Earth - Sun RTBP, where the perturbation depends on three parameters (β, α, δ). Taking Eqs. (2) and (3) we can rewrite Eq. (1) as:

$$\begin{aligned}
\ddot{x} - 2\dot{y} &= \frac{\partial \Omega}{\partial x} + \beta \frac{1-\mu}{r_{ps}^2} \cos^2\alpha \left(\frac{-(x-\mu)z}{r_2 r_{ps}} \sin\alpha\cos\delta + \frac{y}{r_2}\sin\alpha\sin\delta \right), \\
\ddot{y} + 2\dot{x} &= \frac{\partial \Omega}{\partial y} + \beta \frac{1-\mu}{r_{ps}^2} \cos^2\alpha \left(\frac{-yz}{r_2 r_{ps}} \sin\alpha\cos\delta - \frac{x-\mu}{r_2}\sin\alpha\sin\delta \right), \\
\ddot{z} &= \frac{\partial \Omega}{\partial z} + \beta \frac{1-\mu}{r_{ps}^2} \cos^2\alpha \left(\frac{r_2}{r_{ps}} \sin\alpha\cos\delta \right),
\end{aligned} \tag{5}$$

where $\Omega(x,y,z) = \frac{1}{2}(x^2+y^2) + (1-\beta\cos^3\alpha)\frac{1-\mu}{r_{ps}} + \frac{\mu}{r_{pe}}$.

As we know, the classical RTBP (no solar sail) is Hamiltonian, but when we include the the perturbation due the solar sail the Hamiltonian structure of the system breaks down. The system is Hamiltonian only for $\alpha = 0$ (i.e., the solar sail perpendicular to the Sun-sail line) and $\alpha = \pm\pi/2$ (i.e., no sail effect) and for $\alpha \neq 0, \delta = 0$ (i.e., the orientation of the solar sail varies vertically with respect to the Sun-sail line) the system is reversible.[3] In these two particular cases, for a fixed sail orientation, we have periodic and quasi-periodic motion around an equilibrium point.[9,10]

One of the interesting properties of Hamiltonian systems is that they possess at least one first integral, i.e., a function that is conserved through time. For the RTBP, the well-known Jacobi constant is a first integral, and it is related to the energy level of the system. This function is usually used to classify regions of possible motion.[5] In the case of the RTBPS, for a fixed sail orientation $\alpha \neq 0$, there is neither a Jacobi constant nor preserved energy level. However, we would like to define a function that allows us to classify the different types of motion.

As in the RTBP, we define the Jacobi function as:

$$J_c = \dot{x}^2 + \dot{y}^2 + \dot{z}^2 - 2\Omega(x,y,z). \tag{6}$$

Notice that if $\beta = 0$ (i.e., no sail) or if $\alpha = 0$ (a sail perpendicular to the Sun-sail line), this function corresponds to the Jacobi constant of the RTBP or RTBPS (Hamiltonian case). For this last case, effectively, the gravitational parameter μ has been changed. If $\alpha \neq 0$ this function will not be constant but it can still be used to classify types of motion,[3,11] or one can try to select a periodic motion for the sail orientation that keeps this function constant.

The variation of this function over time is computed by substituting Eq. (5) into the time derivative of Eq. (6), having:

$$\frac{dJ_c}{dt} = \beta \frac{1-\mu}{r_{ps}^2} \cos^2\alpha \sin\alpha \left(\frac{\dot{x}y - \dot{y}(x-\mu)}{r_2} \sin\delta + \frac{r_2^2\dot{z} - ((x-\mu)\dot{x} + y\dot{y})z}{r_{ps} r_2} \cos\delta \right). \tag{7}$$

This equation gives an idea on how the energy of the system varies. Notice that, as expected, J_c is constant for $\alpha = 0$ or $\beta = 0$, and for $\alpha \approx 0$ this variation will be small. Moreover we can use Eq. (6) to decide if a transfer trajectory between two regions in the phase space is feasible by checking if its drift in energy is consistent with the predicted rates of variation using Eq. (7). But this is beyond the scope of this paper and is left for future work.

As a final remark, let us mention that the RTBPS satisfies the following symmetries:

$$\begin{array}{l} S1 : (t,\ X,\ Y,\ Z,\ \alpha,\ \delta) \mapsto (-t,\ X,\ -Y,\ -Z,\ -\alpha,\quad \delta), \\ S2 : (t,\ X,\ Y,\ Z,\ \alpha,\ \delta) \mapsto (-t,\ X,\ -Y,\quad Z,\quad \alpha,\ -\delta). \end{array} \tag{8}$$

We can take advantage of these symmetries to compute equilibrium points and to describe the dynamics. For instance, if (x_0, y_0, z_0) is an equilibrium point for the sail orientation (α_0, δ_0), then $(x_0, -y_0, -z_0, -\alpha_0, \delta_0), (x_0, -y_0, z_0, \alpha_0, -\delta_0)$ and $(x_0, y_0, -z_0, -\alpha_0, -\delta_0)$ are also an equilibrium point.

FAMILIES OF EQUILIBRIUM POINTS

It is well known that when we discard SRP ($\beta = 0$) the Earth-Sun RTBP has five equilibrium points,[5] and that all of them lie on the ecliptic plane ($Z = 0$). Three of them, known as the *collinear points* $L_{1,2,3}$, lie on the line joining the two primaries ($Y = 0$). The other two, known as the *triangular points* $L_{4,5}$, lie on the ecliptic plane forming an equilateral triangle with the two primaries (i.e. their distance to both Earth and Sun is 1 AU). The tree collinear points are all linearly unstable (saddle×center×center), and the two triangular points are linearly stable (center×center×center).

If the sail is perpendicular to the Sun-sail line ($\alpha = 0$) the system presents a similar phase space portrait as for $\beta = 0$. There are also have five equilibrium points $SL_{1,\ldots,5}$ on the ecliptic plate, siblings to the classical $L_{1,\ldots,5}$ but displaced towards the Sun.[7] This is because the extra acceleration of the solar sail counteracts a part of the Sun's gravitational attraction. Three of them are collinear points ($SL_{1,2,3}$), since they still lie on the Earth-Sun line; and are still linearly unstable (saddle×center×center). The other two triangular points ($SL_{4,5}$) no longer form an equilateral triangle. Their distance to the Earth is 1 for all $\beta > 0$, but the distance to the Sun behaves as $(1-\beta)^{1/3}$. Both, $SL_{4,5}$ remain linearly stable for all β. We recall that, there is no explicit expression for the collinear equilibrium points, but their distance to the closest primary can be found by solving a quintic equation.[5,7] On the other hand, there is an explicit expression for the triangular points:

$$SL_{4,5} = (x_{4,5}, y_{4,5}, 0) := \left(\mu - \frac{(1-\beta)^{2/3}}{2}, \pm(1-\beta)^{1/3} \left[1 - \frac{(1-\beta)^{2/3}}{4} \right]^{1/2}, 0 \right). \tag{9}$$

When we change the sail orientation ($\alpha \neq 0$ or/and $\delta \neq 0$) we artificially displace the position of the equilibrium points. If we take $\delta = \pm\pi/2$ and vary α we displace the equilibrium points to one side or the other of the Sun-sail line inside the ecliptic plane; while if we take $\delta = 0, \pi$ and vary α we displace the equilibrium points above or below the ecliptic plane, keeping $y = 0$ for each point. Taking any other fixed value of $\delta = \delta^*$ and varying α we displace the equilibrium points on an inclined plane with respect to the ecliptic containing L_i and SL_i.[3,12,13]

For small β ($< 10^{-6}$) we have five disconnected families of equilibrium points, each family being parametrized by the two angles defining the sail orientation. As β grows ($\approx 5.5 \times 10^{-6}$) the equilibria surfaces related to SL_3, SL_4 and SL_5 merge into each other, giving rise to three disconnected families of equilibria (2 spheres one containing SL_1 and the other SL_2, and a banana-like shape surface containing $SL_{3,4,5}$). Between $\beta = 0.02$ and 0.03 the surface related to SL_1 merges with the large surface containing $SL_{3,4,5}$, and after this there are only two remaining families of equilibria (a sphere containing SL_2, and a torus containing the other 4 points). The two remaining surfaces will never merge into each other: the fact that $\langle \vec{n}, \vec{r_s} \rangle > 0$ delimits the regions where there

can be equilibria, separating the SL_1 and SL_2 families.[7,12] Figure 2 shows slices of these surfaces on the $Z = 0$ plane for $\beta = 2 \cdot 10^{-6}, 5 \cdot 10^{-6}, 6 \cdot 10^{-6}, 10^{-3}, 0.01$ and 0.05. Figure 3 shows the behavior of these families for $\beta = 0.01, 0.02$ and 0.03 close to the libration points L_1 and L_2.

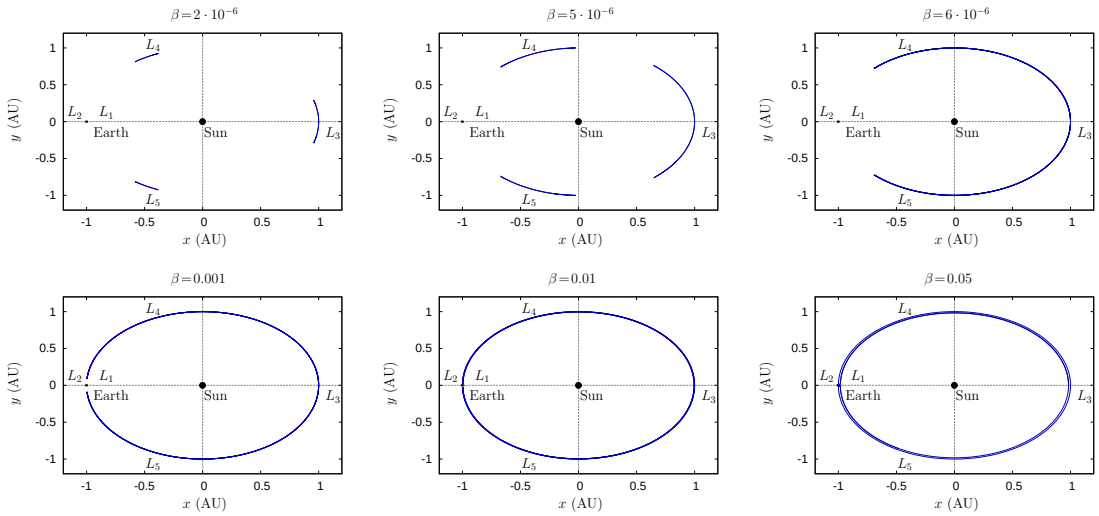

Figure 2. Family of artificial equilibrium points on the xy-plane ($\delta = -\pi/2$) for $\beta = 2 \cdot 10^{-6}, 5 \cdot 10^{-6}, 6 \cdot 10^{-6}, 10^{-3}, 0.01$ and 0.05.

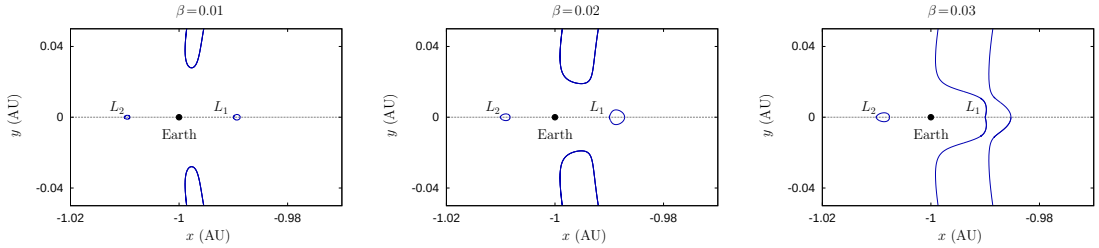

Figure 3. Family of artificial equilibrium points on the xy-plane ($\delta = -\pi/2$) for $\beta = 0.01, 0.02$ and 0.03. Zoomed area close to L_1 and L_2

These families of equilibrium points have been computed using a continuation method using the sail orientation (α) as a continuation parameter. For a fixed of $\beta = \beta^*$ we have started from either: L_i with $\alpha = \pm\pi/2$ or SL_i with $\alpha = 0$, $i = 1, \ldots, 5$. In this study we focus on the dynamics on the ecliptic plane. Hence, in all our computations we have considered $\delta = -\pi/2$, since doing so ensures that the continuation procedure gives equilibria on the xy-plane. Recall that other values of δ would give equilibria outside the ecliptic plane.

For each computed equilibrium point in each family we computed the required sail orientation (α) and its stability. This allows to study what happens before, at and after a collision between two different families of equilibria, as is the case of SL_3 merging into SL_4 and SL_5 for $\beta \approx 5.5 \times 10^{-6}$, and SL_1 merging into SL_4 and SL_5 for $\beta \approx 0.0236$. In terms of the stability we have a family of equilibrium points with two pairs of complex and a pair of real eigenvalues (SL_1 and SL_3) that merge into a family with three pairs of complex eigenvalues (SL_4 and SL_5). In terms of the sail orientation, when two families merge there are sail orientations that are lost. This is illustrated in Figure 4. By this we mean that the equilibria can disappear for certain values of α.

Let us explain this in more detail. First consider β small enough so that the SL_3 family has not yet merged with SL_4 and SL_5 families (e.g. $\beta < 5.5 \times 10^{-6}$). In this case, starting a continuation procedure from $\alpha = 0$ (where all three equilibria $SL_{3,4,5}$ exist) gives rise to three distinct curves, defined for all $\alpha \in [-\pi/2, \pi/2]$. Hence, for each $\alpha \in [-\pi/2, \pi/2]$ all three equilibria exist at the same time. This can be seen in Figure 4, left: the blue curves correspond to the value $\beta = 5 \times 10^{-6}$. Notice that there are three of these curves, where the top, middle, bottom curves correspond to the SL_4, SL_3 and SL_5 families of equilibria, respectively.

When β increases, the amplitude of the corresponding curves also increases, and for $\beta \approx 5.5 \times 10^{-6}$ these three curves collide. After the collision, the three curves have turning points and are not defined in some ranges of α. This situation is that portrayed by the pink lines also in left hand side of Figure 4, that correspond to $\beta = 6 \times 10^{-6}$. Notice that, for this value of β, as α changes from $-\pi/2$ to $\pi/2$, there are situations where there are three, two or even one single equilibrium point (among $SL_{3,4,5}$) in contrast with smaller values of β, where all $SL_{3,4,5}$ exist for all values of α at the same time.

A similar phenomenon happens when the SL_1 family merges with the SL_4 and SL_5 families for β between 0.02 and 0.03 as can be seen on the right plot of Figure 4.

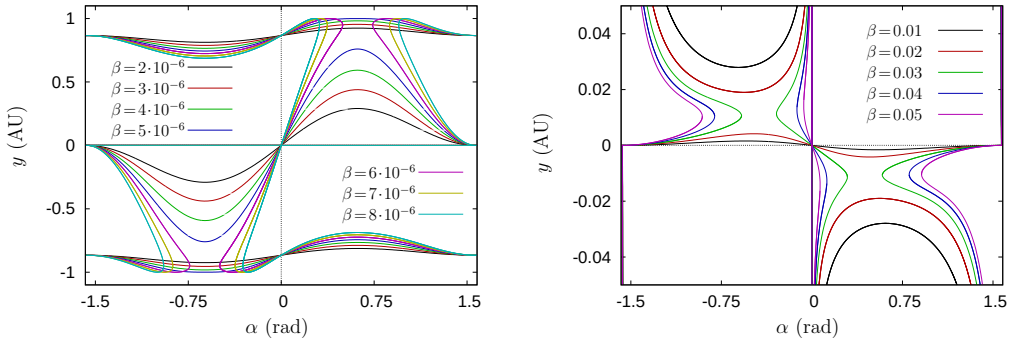

Figure 4. For different values of β, relationship between the y coordinate of the equilibrium point and the sail orientation α.

A general idea of the relation between the position of the equilibrium points and the sail orientation is portrayed in Figure 5. The two plots on the left hand side of Figure 5 show the different families of equilibrium points for $\beta = 0.01, 0.02, 0.03, 0.04$ and 0.05 near to Earth (top) and close to L_4 (bottom), and different colors represent different values of β. The two plots on the right hand side of Figure 5 show the same equilibrium points but now the color coding (right palette) represents the required sail orientation α to have equilibria. As we can see the, equilibria in the family L_2 have the full range of sail orientation ($\alpha \in [-\pi/2, \pi/2]$) while the equilibria close to L_1 and L_4 are restricted to sail orientations $\alpha \approx \pm\pi/2$ or $\alpha \approx 0$.

Let us now briefly discuss the stability of the different families of equilibrium points, which is given by the eigenvalues of the linearized flow around the equilibrium points. As we have mentioned in the previous section, the system is only Hamiltonian for three distinctive values of the sail parameters, $\alpha = 0$ (i.e. sail perpendicular to Sun-satellite line) and $\alpha = \pm\pi/2$ (i.e. sail aligned with Sun-satellite line, hence no sail effect). For the rest of the sail's parameters the system is only divergence free, which means that the trace of the monodromy matrix is zero and so is the sum of the eigenvalues.

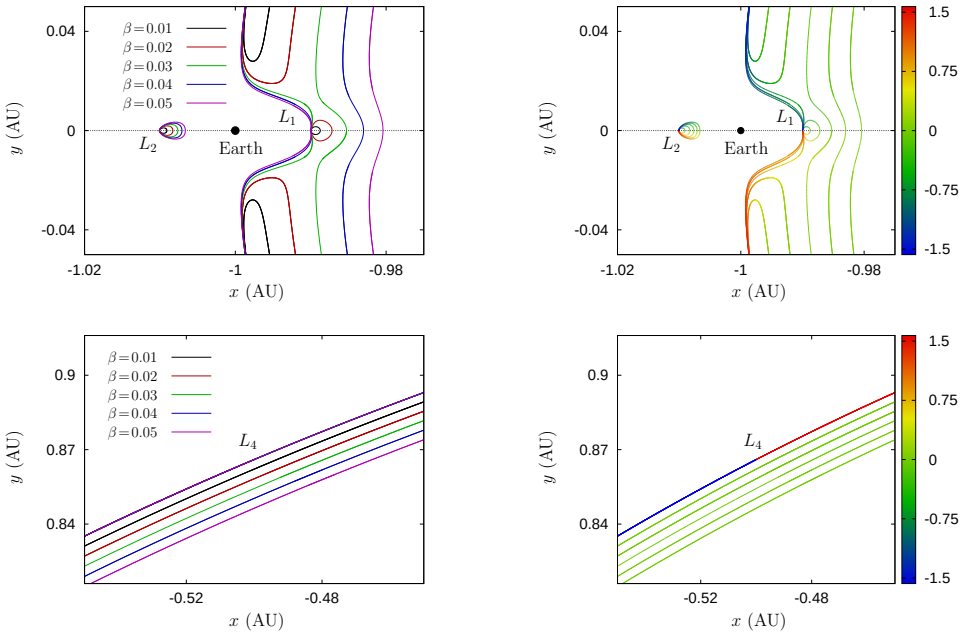

Figure 5. Families of equilibrium points for $\beta = 0.01, 0.02, 0.03, 0.04$ and 0.05 in the vicinity of L_1 and L_2 (top) and the vicinity of L_4 (bottom). Left: the families are grouped by colors depending on the value of β. Right: the families are grouped by colors depending on the sail orientation α.

We recall that in Hamiltonian systems, the eigenvalues of the linearized flow come in pairs, i.e., if λ is an eigenvalue, then $-\lambda$ and $\bar{\lambda}$ must also be eigenvalues. But this is not true when the system is no longer Hamiltonian. In the RTBPS the we distinguish between two classes of equilibrium points. The first class, $\mathcal{T}_1$, of unstable equilibria, whose eigenvalues are $\lambda_1 > 0, \lambda_2 < 0, \nu_1 \pm \mathtt{i}\omega_1$ and $\nu_2 \pm \mathtt{i}\omega_2$. Here $|\nu_{1,2}| \ll |\lambda_{1,2}|$ and hence, the main instability is given by the saddle. The second class, $\mathcal{T}_2$, are equilibria whose all eigenvalues are complex $\nu_{1,2,3} \pm \mathtt{i}\omega_{1,2,3}$. Concerning the equilibria close to L_4 and L_5, we can see that $|\nu_{1,2,3}| < 0.001$ and we can refer to these equilibrium points as practically stable in the sense that the required time to leave the vicinity of the equilibrium point is large (i.e., it would take more that 110 years to double the initial distance from the equilibrium point). Figure 6 shows the relation between the position of the equilibrium point and the class they belong to for different values of β. We can see that the equilibria close to L_1, L_2 and L_3 are unstable change to practical stable points as they get close to L_4 and L_5.

We note that for the equilibrium points that lie on the xy-plane (i.e. $\delta = -\pi/2$) of any of the two classes $\mathcal{T}_1$ and $\mathcal{T}_2$, one of the complex eigenvalues is related to the vertical oscillation and the real part of this pair of eigenvalues is always zero. As mentioned above, the equilibria close to L_1 and L_2 are of class $\mathcal{T}_1$, and on the xy-plane their eigenvalues are such that $\lambda_1 > 0, \lambda_2 < 0, \nu_1 \pm \mathtt{i}\omega_1, \pm\mathtt{i}\omega_2$. For $\alpha > 0$ we have that $\nu_1 > 0$ and for $\alpha < 0$, $\nu_1 < 0$. Moreover, $\lambda_1 + \lambda_2 + 2\nu_1 = 0$. This can be seen in Figure 7 where we plot the relation between the equilibria location and the sign of α and the values of the pair of real and complex eigenvalues (top: $\beta = 0.01$ and bottom: $\beta = 0.03$). Note that we do not plot the complex eigenvalue related to the vertical oscillation (ν_2).

If we focus on the equilibria close to L_4 and L_5 on the plane, we have that the eigenvalues are $\nu_1 \pm \mathtt{i}\nu_1, \nu_2 \pm \mathtt{i}\nu_2$ and $\pm\mathtt{i}\nu_3$. Since the sum of the eigenvalues has to be zero, we have that

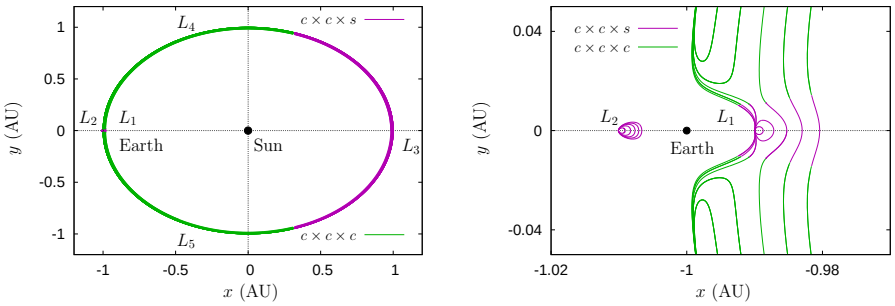

Figure 6. Stability indicator for the family of equilibrium points on the xy-plane ($\delta = -\pi/2$) for $\beta = 0.01, 0.02, 0.03, 0.04$ and 0.05. The class $\mathcal{T}_1$ and $\mathcal{T}_2$ are represented in color purple and green respectively. Right: Zoom close to L_1 and L_2.

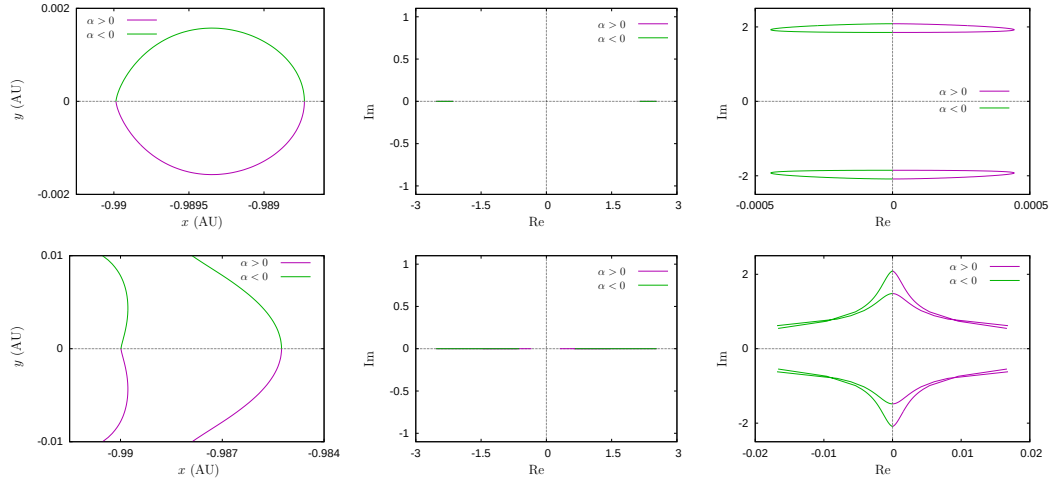

Figure 7. L_1 family of equilibria on the xy-plane for $\beta = 0.01$ (top), $\beta = 0.03$ (bottom). Purple lines correspond to $\alpha > 0$ and green lines to $\alpha < 0$. Left: xy position of the equilibria. Middle: real eigenvalues λ_1, λ_2. Right: complex eigenvalue $\nu_1 \pm \mathtt{i}\omega_1$.

$\nu_1 + \nu_2 = 0$, hence $\nu_1 \cdot \nu_2 < 0$. This means that there is a plane in the phase space where the system is dissipative and another plane where the dynamics is attracting, and these two phenomena occur at a very small rate as $|\nu_i| < 5 \times 10^{-6}$. This can be seen in Figure 8 for the L_4 (top) and L_5 (bottom) and $\beta = 0.01$. As in the previous case, on the left of Figure 8 we have the relation between the equilibria location of sign of α, where we can appreciate the symmetries of the system between L_4 and L_5. On the middle and right hand side of the Figure we show the two pair of complex eigenvalues $\nu_1 \pm \mathtt{i}\nu_1, \nu_2 \pm \mathtt{i}\nu_2$ and we can see how for both ($\alpha > 0$ and $\alpha < 0$) if $\nu_1 > 0$ then $\nu_2 < 0$ and vice versa. We must mention that these equilibrium points are not a true complex saddle as the frequencies related to each of the eigenvalues is different ($\omega_1 \neq \omega_2$).

These equilibrium points have been proposed as target positions for several mission applications,[12] the most relevant ones are the SunJammer and the Polar Observer missions. But they require to remain close to an equilibrium point from the L_1 and L_2 families which are unstable and require station keeping maneuvers to remain close to them. We propose the focus on the regions close to L_4 and L_5 for potential destinations of our sailcraft and use the invariant manifolds related to L_1 and L_2 to reach this regions. Preliminary studies in this direction can be found in the literature

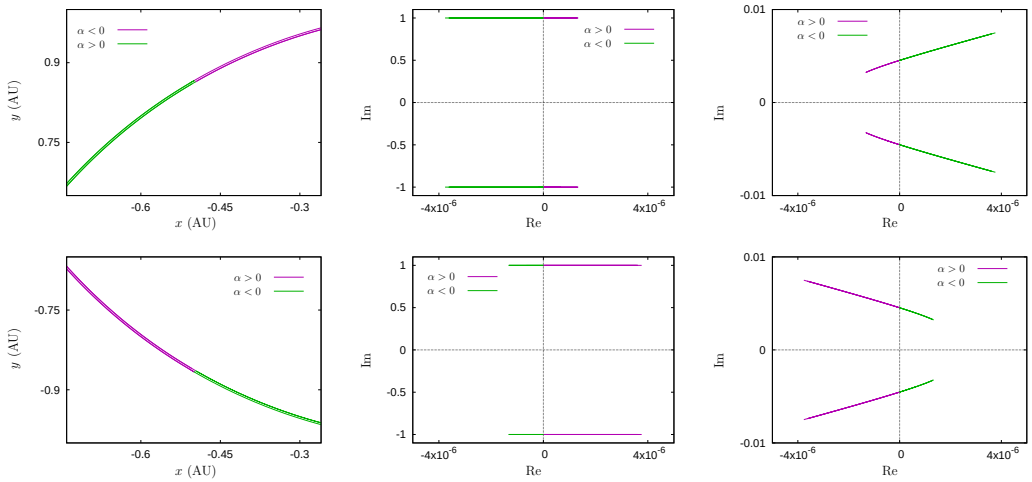

Figure 8. Family of equilibria at L_4 (top) and L_5 (bottom) on the xy-plane for $\beta = 0.01$. Purple lines correspond to $\alpha > 0$ and green lines to $\alpha < 0$. Left: xy position of the equilibria. Middle: first pair of complex eigenvalues $\nu_1 \pm \mathtt{i}\omega_1$. Right: second pair of complex eigenvalues $\nu_2 \pm \mathtt{i}\omega_2$.

and show promising results. One interesting mission application would be to place two sailcrafts, one at SL_4 and the other at SL_5 in order to monitor the Sun's activity free of inferences. Using any of the existing Sun observers at L_1 with the two satellites at SL_4 and SL_5 we could monitor the activity of the Sun from three distinct vantage points. A constellation of this nature could track the evolution of sunspots or geomagnetic storms, helping to develop a better understanding of the Sun's activity.

In this paper we want to focus on describing the natural dynamics of a solar sail around L_4 and L_5. In the next section we describe the regions of practical stability that appear around both points and how they vary when we change some of the sail parameters. We also discuss the type of motions that appear there. The study on how to reach these regions from the collinear points is left for future work.

REGION OF PRACTICAL STABILITY AROUND L_4/L_5

As explained above, it is well known that if we neglect the SRP (i.e., $\beta = 0$), the triangular Lagrangian points L_4 and L_5 of the RTBP are linearly stable. When the effect of the sail is added (i.e., $\beta > 0$), if the orientation of the sail is perpendicular to the Sun-sail line (i.e., $\alpha = 0$) the RTBPS is still Hamiltonian and the $L_{4,5}$ siblings ($SL_{4,5}$) are still linearly stable. Hence, when $\alpha = 0$ we expect to find a region of practical stability in a vicinity of these points.

By region of practical stability we refer to a set of initial conditions with zero synodical velocity $\dot{x} = \dot{y} = \dot{z} = 0$ close to $SL_{4,5}$ that remain close this point after $T > 0$ years. This requires to establish an escaping criterion. From the mathematics perspective, such a region is defined as the set of initial conditions inside a compact vicinity K of $SL_{4,5}$ that do not leave a larger set $K' \supset K$ in less than $T > 0$ years. In particular, crossing the boundary of the set K' is precisely the escaping criterion. The way we choose K and K' in the present problem is stated in the next subsection, devoted to explain the method used to find this region.

Referring to this region as of practical (or effective) stability comes from the theory of Hamil-

tonian dynamical systems in three or more degrees of freedom, as the spatial RTBP is. In such systems, around linearly stable points, one always expects Arnol'd diffusion to take place. In our setting for $\beta = 0$ and $\beta > 0, \alpha = 0$ we expect an exponentially slow drift of initial conditions around $L_{4,5}$ or $SL_{4,5}$, so it may happen that orbits that are confined for thousands of years in a vicinity of these points will eventually escape but after an exponentially long time span. For instance, if we consider the spatial RTBP for the system Sun-Jupiter, there is an stability region around L_4 of the order of magnitude of kilometers where initial conditions remain close to L_4 over a time interval of about $2 \cdot 10^{10}$ years.[14] This region is, in fact, where the Trojan asteroids are found and this phenomenon explains why these asteroids remain in that position. Such slow drift will not be noticeable in the time span of the missions to $SL_{4,5}$ we are interested in.

As explained above, for $\alpha \neq 0$, the equilibria $SL_{4,5}$ have some attracting/dissipative directions. Hence, one expects that the initial conditions that remained close to $SL_{4,5}$ for $\alpha = 0$ will escape after a short time. Yet when α is small enough, the attraction/dissipation is weak and some remnant of this region is still detectable. For our purposes, we are interested in the set of initial conditions that subsist close to $SL_{4,5}$ for more than $T = 1000$ years.

The region of practical stability we are dealing with is a actually 3D set (recall that we consider zero synodical velocity), but we are going to restrict ourselves in the dynamics on the ecliptic plane $z = 0$. Hence, we are only going to study a slice of the complete set. In Simó[15] the author shows some examples of this 3D region for the spatial RTBP. From now on, we will refer to the intersection of the set of practical stability surrounding $SL_{4,5}$ with $\{z = 0\}$ as $\mathcal{A}^T_{\alpha,\beta}$.

The goal of this section is to characterize $\mathcal{A}^T_{\alpha,\beta}$ for values $\beta = 0.01, 0.02, 0.03, 0.04$ and 0.05, $\alpha = 0$ and α small and $T > 0$.

A method to approximate $\mathcal{A}^T_{\alpha,\beta}$

We have used the method proposed by Simó et. al[16] to approximate $\mathcal{A}^T_{\alpha,\beta}$. In this subsection we briefly outline this method. To fix ideas, we restrict ourselves to the region that surrounds SL_4. The corresponding region around SL_5 can be obtained by means of the symmetries of Eq. (8). Recall that one can give an explicit expression of the coordinates of SL_4 as a function of β, see Eq. (9). Recall also that its distance to the Sun is $(1 - \beta)^{1/3}$, so it approaches the position of the Sun as $\beta \to 1$. The dotted blue line in Figure 9 shows the position of SL_4 for different values of $\beta \in [0, 1]$.

To obtain a good approximation of the region of practical stability we should change to a suitable system of coordinates. Due to the shape the set $\mathcal{A}^T_{\alpha,\beta}$ has in synodical coordinates, it is convenient to choose polar coordinates centered at the Sun,[4] see Figure 9 top left. A translation allows to put SL_4 in the origin of these polar coordinates. We consider the variables $(r, \theta) \in (-(1-\beta)^{1/3}, \infty) \times [-0.5, 0.5)$ (measured in AU and rad/(2π), respectively) defined as the distance to SL_4 and the angle with respect to the SL_4-Sun line, respectively. Hence,

$$x = \mu + (r + r_4)\cos(2\pi\theta + \theta_4), \quad y = (r + r_4)\sin(2\pi\theta + \theta_4) \tag{10}$$

where $r_4 = \sqrt{(x_4 - \mu)^2 + y_4^2}$ and $\theta_4 = \arctan(y_4/(x_4 - \mu))$ the polar coordinates of SL_4, see Eq. (9).

In the following we will study $\mathcal{A}^T_{\alpha,\beta}$ in the coordinates (r, θ). The method consists of two steps. The first step consists in performing a brute-force integration of initial conditions chosen close to SL_4. The second step consists in refining the previous approximation by means of integrating the initial conditions in the boundary for larger times.

Step 1: First approximation Consider a box $K = [\theta_0, \theta_1] \times [r_0, r_1]$ and a $N_\theta \times N_r$ equispaced grid on it. First fix a number of years, say $T_0 > 0$. Each point in the grid (θ_i, r_j) (or pixel), where

$$\begin{aligned} \theta_i &= \theta_0 + i(\theta_1 - \theta_0)/(N_\theta - 1), \qquad i = 0, \ldots, N_\theta - 1, \\ r_j &= r_0 + j(r_1 - r_0)/(N_r - 1), \qquad j = 0, \ldots, N_r - 1, \end{aligned}$$

corresponds to an initial condition for the integration of Eq. (1) where x, y are obtained via Eq. (10), $z = 0$ and $\dot{x} = \dot{y} = \dot{z} = 0$. Each initial condition is integrated until at most $t = 2\pi T_0$. We distinguish between escaping and subsisting initial conditions.

The *escaping criterion* is that for some $t < 2\pi T_0$, $y < -0.5$. Hence $K' = \{y \geq 0.5\}$. Escaping orbits are labeled in the grid by -1, and all initial conditions that do not leave K' after T_0 years are labeled with a $+1$ in the grid. The latter constitute the first approximation of the region of practical stability, $\mathcal{A}^{T_0}_{\alpha,\beta}$.

Step 2: Refinement The refinement consists in re-iterating the boundary of the previously approximated region for a larger number of revolutions. We call the boundary of depth d, $d = 1, 2, 3, \ldots$ to the set of all pixels (r_j, θ_i) previously labeled with a 1 such that at least one pixel (r_{j+m}, θ_{i+n}), $n, m = -d, -d+1, \ldots, d-1, d$ is labeled with a -1.

After setting $T_1 > T_0$, all the pixels in the boundary of depth d are re-integrated until $t = 2\pi T_1$ and classified (and labeled) as either escaping or non-escaping according to the previous criterion. After this, the boundary may have changed, and it is re-checked using the same procedure until none of the pixels of the boundary escape before T_1 years. The refinement process can be repeated as many times as desired.

The value of the depth d has to be chosen accordingly to the rate of escape of orbits and the maximal number of years we integrate. Here, for the Hamiltonian cases we have used $d = 2$ and for the non-Hamiltonian cases $d = 5$. This avoids having to re-check the boundary many times in case one knows a priori that orbits escape fast.

Other observables There are some measurable quantities that are of interest for our purposes. We denote

$$A^T_{\alpha,\beta} = \text{Area}\left(\mathcal{A}^T_{\alpha,\beta}\right),$$

the size of the region of practical stability in polar coordinates (r, θ).

Apart from describing and measuring $\mathcal{A}^T_{\alpha,\beta}$, we are also interested in the kinds of motion the orbits in this set experience. To have a first idea of the type of trajectories we are dealing with, we are going to measure, along trajectories that start at points in $\mathcal{A}^T_{\alpha,\beta}$ how much do the polar coordinates (r, θ) vary. To do so, we integrate each initial condition in $\mathcal{A}^T_{\alpha,\beta}$ for $T_0 \leq T_1$ years keeping track on its position in the polar coordinates r and θ. In the course of integration, we save the maximal and minimal values they attain, denote them by $r_{\max}$, $r_{\min}$, $\theta_{\max}$ and $\theta_{\min}$. To study the kinds of motion inside $\mathcal{A}^T_{\alpha,\beta}$ we compute, for each trajectory, the quantities

$$\begin{aligned} \Delta r &= r_{\max} - r_{\min}, \\ \Delta\theta &= \theta_{\max} - \theta_{\min}. \end{aligned}$$

Note that this gives a measure of the maximal distance of the trajectories to $SL_{4,5}$ that start close to these equilibria.

A numerical study of the regions of practical stability

Here we describe the numerical results concerning the region $\mathcal{A}^T_{\alpha,\beta}$, mainly concerning its shape and area and how they vary as a function of the parameters α and β. The results shown can be separated in two distinct parts. First, we will deal with the Hamiltonian case $\alpha = 0$, by studying the shape and area of $\mathcal{A}^T_{\alpha,\beta}$, and how do these sets vary as β increases. Second, we will study the case $\alpha \neq 0$. Namely if the structures observed for $\alpha = 0$ are preserved for $\alpha \neq 0$. Special emphasis will be made in the previous description of the evolution of the families of equilibria $SL_{1,2,3,4,5}$.

The Hamiltonian case $\alpha = 0$. Evolution of $\mathcal{A}^T_{\alpha,\beta}$ as a function of β The first results concern the case when the sail is perpendicular to the Sun-sail line ($\alpha = 0$). For all the computations performed for this case the maximal number of revolutions is $T_1 = 10^4$, and the size of the grid was $N_\theta = N_r = 1000$. It is worth noting that the differences with the results obtained by taking $T_0 = 10^3$ are negligible.

The main features of $\mathcal{A}^{T_1}_{0,\beta}$ we want to highlight are summarized in Figure 9. In the top left plot we display $\mathcal{A}^{T_1}_{0,\beta}$ for $\beta = 0.01, 0.02, 0.03, 0.04$ and 0.05 in synodical coordinates x and y. As we can see, the displayed regions are very narrow. Also, since SL_4 approaches the Sun as β increases, so do the regions $\mathcal{A}^{T_1}_{0,\beta}$.

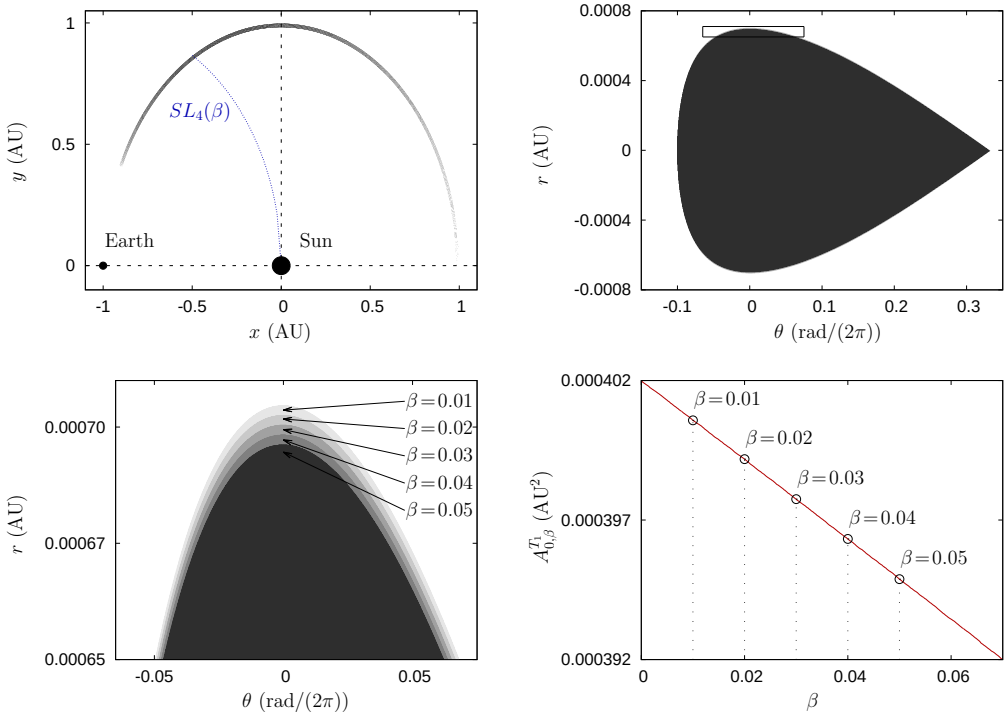

Figure 9. Evolution of the practical stability region for $T_1 = 10^4$ revolutions. Top left: $\mathcal{A}^{T_1}_{0,\beta}$ for $\beta = 0.01, \cdots, 0.05$ in the xy variables. The dotted blue line shows the position of SL_4 for $\beta \in [0, 1]$. Top right: Same as top left in the (r, θ) variables, see Eq. (10). Bottom left: Magnification of the square in the top right picture. Bottom right: Evolution of the area $A^{T_1}_{0,\beta}$ as a function of $\beta \in [0, 0.07]$.

In Figure 9 top right, we see the same regions as in the top left plot, but in the polar coordinates (r, θ), see Eq. (10). Recall that in these variables, the origin corresponds to SL_4. These coordinates

are suitable to compare the regions with each other. The shape of $\mathcal{A}^{T_1}_{0,\beta}$ is characteristic of its analogue of the spatial RTBP for small values of μ.[15,16] It seems that as β increases, the area $A^{T_1}_{0,\beta}$ of $\mathcal{A}^{T_1}_{0,\beta}$ decreases. In Figure 9, bottom left we show a magnification of the squared region of the top right plot. This magnification shows how does $\mathcal{A}^{T_1}_{0,\beta}$ change for the different values of β. Namely, the region becomes narrower in the r variable. In the θ variable, it seems that the region slightly moves towards positive values of θ. This can be seen in extended computations. In the bottom right plot we show how the area $A^{T_1}_{0,\beta}$ varies as a function of $\beta \in [0, 0.07]$: in this range it seems that the region decreases linearly. Extended computations for larger values of β show that the global behavior is not linear.

The Hamiltonian case $\alpha = 0$. Oscillations of orbits: the observables Δr and $\Delta\theta$ of orbits starting in $\mathcal{A}^{T_1}_{0,\beta}$ In synodical coordinates x, y some trajectories that start at $\mathcal{A}^{T_1}_{\alpha,\beta}$ elongate on an annulus centered in the position of the Sun and covers a wide range of angles $\theta \in [-0.1, 0.35]$ rad/(2π) measured from $SL_4(\beta)$. This ranges most of the upper half-plane. One expects that the closer we start from SL_4, less would the magnitude of Δr and $\Delta\theta$ be. From the point of view of applications it may be of interest to put a probe in some subset of this region where the oscillations are bounded in some prescribed interval.

We have computed Δr and $\Delta\theta$ for all the initial conditions in $\mathcal{A}^{T_1}_{0,\beta}$ integrating them for $T = T_0 = 10^3$ years. At the used resolution level, in all five cases $\beta = 0.01, 0.02, 0.03, 0.04$ and 0.05 the oscillations ranged $\Delta r \in [0, 0.01]$ and $\Delta\theta \in [0, 0.45]$ and distribution of Δr and $\Delta\theta$ in the domains $\mathcal{A}^{T_1}_{0,\beta}$ looked all qualitatively the same. As an example, we display the case $\beta = 0.03$ in Figure 10. On the left, we show the distribution of Δr and on the right we show the distribution of $\Delta\theta$. Each shade of gray corresponds of an interval of Δr or $\Delta\theta$: The subsets labeled with $i = 1, \ldots, 6$ correspond to initial conditions for which $\Delta r \in [(i-1)\cdot 0.0017, i \cdot 0.0017)$ and $\Delta\theta \in [(i-1)\cdot 0.075, i \cdot 0.075)$.

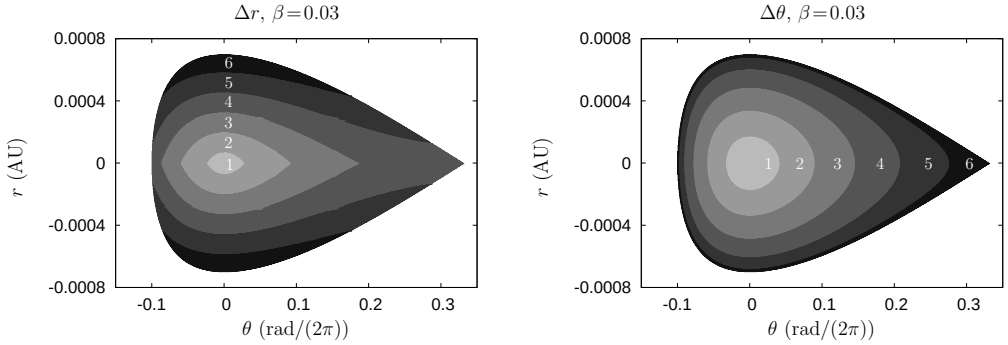

Figure 10. Region $\mathcal{A}^{T_1}_{0,0.03}$ for $T_1 = 10^4$ in polar coordinates. Left: Δr. Right: $\Delta\theta$.

For both observables, the initial conditions that have smaller values of Δr and $\Delta\theta$ are those closer to SL_4. These are the lightest regions in both plots, labeled with a 1. Concerning Δr, the initial conditions that have larger values are those that are farther from SL_4 in the r variable. See the region labeled with a 6 in the left plot of Figure 10. On the other hand, the largest values of $\Delta\theta$ are attained at the boundary of the region $\mathcal{A}^{T_1}_{0,\beta}$, see the region labeled with a 6 in the right plot of Figure 10.

In Figure 10 we have shown qualitatively how the oscillations vary in the regions $\mathcal{A}^{T_1}_{0,\beta}$, but it is

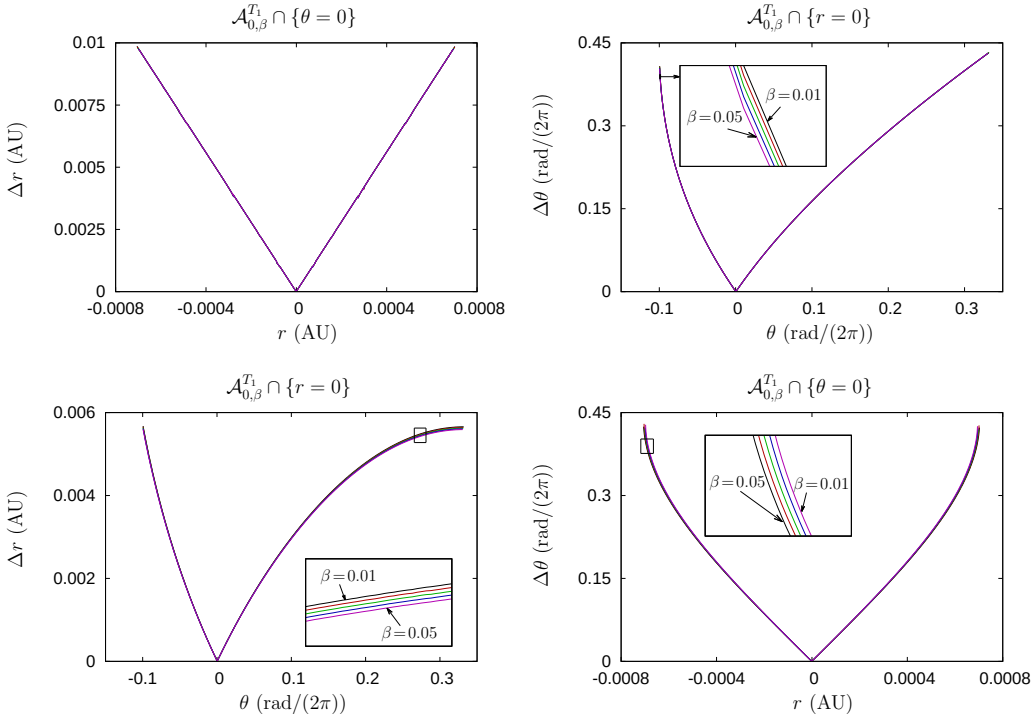

Figure 11. For $\beta = 0.03$. Left (resp. right): Variation of Δr (resp. $\Delta\theta$) along the line $\{\theta = 0\}$ (top) and $\{r = 0\}$ (bottom) (resp. $\{r = 0\}$ (top) and $\{\theta = 0\}$ (bottom)).

important to notice that the magnitudes Δr and $\Delta\theta$ vary continuously along any line that crosses the region of practical stability. In Figure 11 left (resp. right) we show how does Δr (resp. $\Delta\theta$) vary along the lines $\{\theta = 0\}$ (top left and bottom right) and $\{r = 0\}$ (top right and bottom left). As expected, these quantities vary continuously and have an absolute minimum at the position of SL_4. In the top left plot we cannot distinguish between the 5 lines that are shown due to the resolution used. But in the other 3 figures, the magnifications show that the oscillations become smaller as β increases.

The non-Hamiltonian case $\alpha \neq 0$. Ranges of α where SL_4 exists The most important feature of the RTBPS for $\alpha \neq 0, \beta > 0$ to be taken into account here is that, as explained in previous sections, for some ranges of α the RTBPS has less than 5 equilibria. In some cases both $SL_{4,5}$ disappear, and so does any region of practical stability in its vicinity.

The SL_4 family has been determined by means of a continuation method in previous sections. In Figure 12 we show continuation curves of the y component of SL_4 with respect to α. This Figure is a magnification close to $\alpha = 0$ of the right plot in Figure 4. The dotted vertical line in the left plot indicates $\alpha = 0$. Its intersection with the five displayed curves are, from top to bottom, SL_4, SL_3 and SL_5. If we restrict ourselves to SL_4, extended computations show that the family can be continued for $\alpha < 0$ for values that exceed $\alpha = \mathcal{O}(10^{-2})$, which is enough for the purposes of this work. But for the displayed values of β, the continuation for $\alpha > 0$ encounters a turning point. These are indicated in the magnification shown in the right plot as α_i, $i = 1, 2, 3, 4, 5$. Approximations of these values are given in Table 2.

These turning points indicate, for each value of β, the precise value of α at which the equilibrium

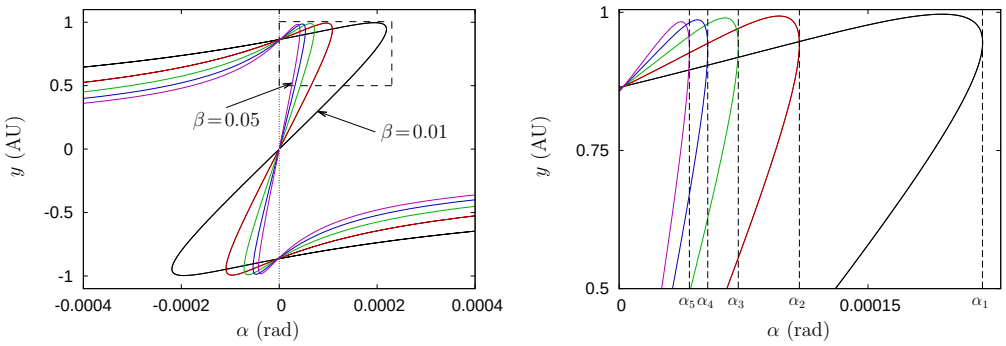

Figure 12. Continuation curves of displaced SL_4 equilibria, y vs α, for $\beta = 0.01, 0.02, 0.03, 0.04$ and 0.05. The curves corresponding to the smallest and largest values of β are indicated in the plot. The right plot is a magnification of the left plot at the dashed square. The abscissas $\alpha_{1,2,3,4,5}$ indicate the turning points location.

Table 2. Value of α for which the continuation of SL_4 increasing α undergoes a turning point.

β	0.01	0.02	0.03	0.04	0.05
α (rad)	$2.1908{\cdot}10^{-4}$	$1.0863{\cdot}10^{-4}$	$7.1816{\cdot}10^{-5}$	$5.3404{\cdot}10^{-5}$	$4.2359{\cdot}10^{-5}$

SL_4 ceases to exist. Hence to study the regions $\mathcal{A}^T_{\alpha,\beta}$ we should only restrict ourselves to values of α that are to the left of the corresponding turning point. Note that the same analysis applies for SL_5 up to a change of sign in α, see Eq. (8).

The non-Hamiltonian case $\alpha \neq 0$. The area of $\mathcal{A}^T_{\alpha,\beta}$. Here we restrict ourselves to a maximal number of revolutions $T = T_0 = 10^3$, a grid size $N_\theta = N_r = 500$, and proceed as before for the Hamiltonian case $\alpha = 0$. We are mainly interested in detecting for which values of α we can find a non-negligible region of practical stability. This is a remnant of the one that appears for $\alpha = 0$.

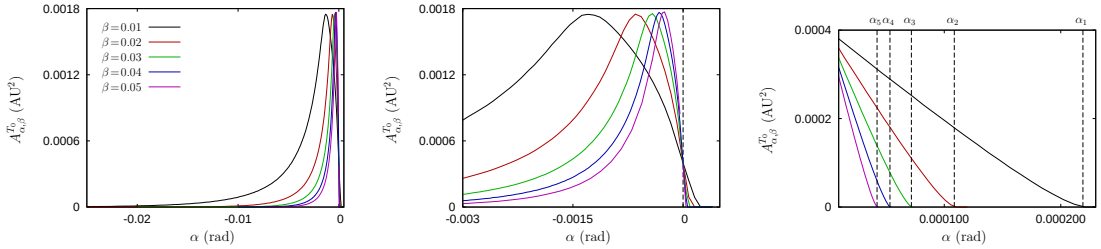

Figure 13. Evolution of the area $A^{T_0}_{\alpha,\beta}$ for $\beta = 0.01, 0.02, 0.03, 0.04$ and 0.05. Left plot: the full range where $A^{T_0}_{\alpha,\beta} > 0$. Middle and right plots are magnifications of the left plot. In the right plot, the values $\alpha_{1,2,3,4,5}$ from Table 2 are indicated.

The main features we highlight about this case are those extracted from the results shown in Figure 13. In the left plot we display the area $A^{T_0}_{\alpha,\beta}$ as a function of α for the 5 values of β indicated in the full range around $\alpha = 0$ where we detected this area. The middle and right plots are magnifications of the left one. In these three plot we observe the following:

1. As β increases, the range of α where $A^{T_0}_{\alpha,\beta}$ is non-negligible shrinks around $\alpha = 0$, see

Figure 13 left and middle.

2. For all displayed values of β, starting at $\alpha = 0$, the area $A^{T_0}_{\alpha,\beta}$ decreases to zero for $\alpha > 0$ (see Figure 13 right) and increases to be more than 4 times larger for $\alpha < 0$ and then decreases back to 0, see Figure 13 middle and left.

3. The disappearance of the region $\mathcal{A}^{T_0}_{\alpha,\beta}$ occurs at the value of $\alpha > 0$ where the continuation of SL_4 for the corresponding value of β has the turning point shown in Figure 12, right.

REACHING THE L_4 AND L_5 STABILITY REGIONS

As mentioned earlier, an interesting mission concept that could take advantage of the L_4/L_5 practical stability regions would be to place simultaneously two satellites (one at L_4 and the other at L_5) to observe the Sun's activity from two different points of view. The final goal of our project is to study the feasibility of such mission concept using a solar sail or a low-thrust propulsion systems.

In the previous section we have discussed the effect of SRP on the practical stability regions around L_4/L_5. As we have seen, when the sail is perpendicular to the Sun-satellite line ($\alpha = 0$) these regions are shifted towards the Sun and their size varies slightly as the sail lightness number (β) increases. When we change the sail orientation, as Figure 13 shows, the total area of the stability region drastically decreases. Note that there is almost no stability region for $|\alpha| > 0.01$ rad.

We have also described the motion inside the stability region in the case $\alpha = 0$. We know that orbits inside this region region experience two kinds of oscillations, one related to the distance to the Sun (Δr), and the other related to the angular variation relative to the L_4-Sun line ($\Delta\theta$). As Figure 10 shows, the sizes of these oscillations become smaller as one gets closer to L_4/L_5. Hence, depending on the mission requirements, one can target a specific location inside the practical stability region. Ideally, in the case of a Sun observer, we want these variations to be small in order to avoid communication problems and to be able to observe at all time the same Sun area.

The access to these regions has always been hard, not only due to the large distance, as they are approximately at 1 AU, but also in terms of the Δv budget. The orbits inside this region can either be trapped or leave a vicinity of it after a long time, which means that it is also hard to get inside without a large Δv maneuver. Recent studies[1,2] show that using a solar sail, we can continuously accelerate the probe in order to reduce the time of flight and final Δv. The main idea is to use the invariant manifolds related to the equilibrium points and periodic orbits related to L_1 and L_2 as transfer orbits to this region. By tilting the sail orientation we can slowly increase the energy of the system (Eq. 7) and reach the orbits in this region. When reaching the region, resetting the sail to $\alpha = 0$ should be enough to get trapped in this region.

To illustrate this we have computed the stable and unstable manifolds related to SL_1 and SL_2 for different values of β. In this way we have an idea of the general trend the invariant manifolds have, and how the size of the solar sail affects them. Figure 14 shows the stable and unstable manifolds for $\beta = 0$ (left), 0.01 (middle) and 0.02 (right). A general view and their relative position with respect to the practical stability region ($A^{T_1}_{0,\beta}$) appears on the top plots. The bottom plots are a zoom close to the Earth. We note that all these invariant manifolds have been computed up to $t_f = 10$ years. Hence, the longer the unstable manifold path is, the faster the transfer to L_4 can be.

It is interesting to note that, for $\beta = 0$ (i.e. no sail), we can only reach L_4 from L_2 and L_5 from L_1. But the extra effect due to the solar sail allows us to reach L_4 and L_5 from L_1. This is very convenient for the mission scenario where we consider two satellites, one aiming to L_4 and the other

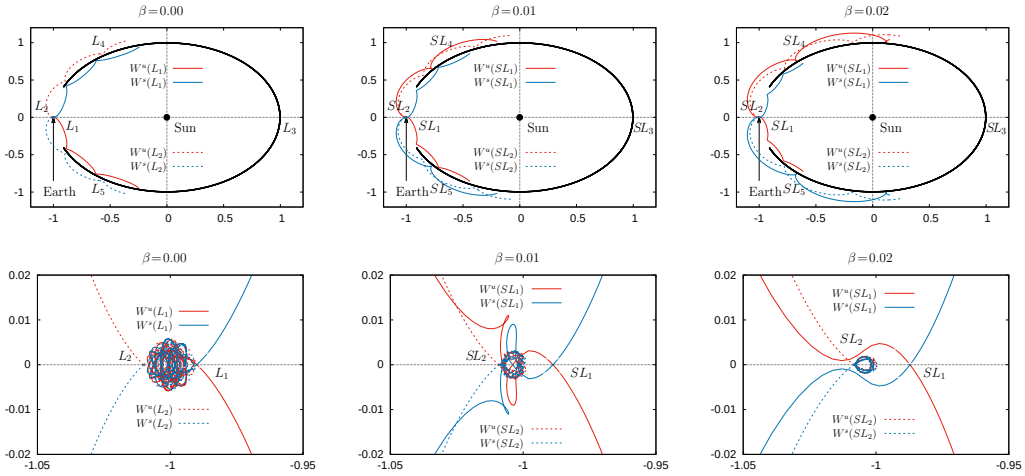

Figure 14. Stable (blue) and Unstable (red) manifolds of SL_1 and SL_2 for $\beta = 0, 0.01$ and 0.02. Top, general view and relation with the practical stability (black). Bottom, zoom of these manifolds close to the Earth.

to L_5, as we could use a same launch vehicle to reach the L_1 invariant manifolds. In the near future we will focus in the design of a transfer strategy and the optimization of the transfer orbits from $L_{1,2}$ towards the practical stability regions around L_4 and L_5.

CONCLUSIONS AND FUTURE WORK

In this paper we have performed a preliminary study of the dynamics of a solar sail in a vicinity the triangular libration points $L_{4,5}$. These fixed points exist for all values of the lightness number (β) if the sail is oriented towards the Sun-sail line ($\alpha = 0$). Moreover, for these values of the parameters, they are linearly stable and exhibit some region of practical stability around them.

We have reviewed the most important properties of the Sun-Earth RTBPS: when $\beta = 0$ or $\alpha = 0$ the system is Hamiltonian, and we have briefly discussed the symmetries and first integrals of the system. When $\beta \neq 0$ and $\alpha \neq 0$, the RTBPS is no longer Hamiltonian and it has a huge impact concerning the existence, position and stability of the equilibria of the system. We have performed a study of the families of equilibria, with special emphasis on determining the ranges of the parameters where $L_{4,5}$ exist, and which is their stability. This study has been crucial to study the regions of practical stability.

We have performed a study of the regions of practical stability: this is a set of initial conditions close to $L_{4,5}$ with zero synodical velocity whose corresponding trajectory remains close to $L_{4,5}$ for at least 1000 years. For $\alpha = 0$ we have described the motion of the trajectories inside this region, by characterizing how further from $L_{4,5}$ they arrived. After that, we have set $\alpha \neq 0$ for the values suggested by the previous study of families of equilibria, and we have determined ranges of $\alpha \neq 0$ where the region of practical stability was non-negligible. This gives an idea of which orientations of the sail are feasible to reach the practical stability region.

We have finished this contribution by suggesting a mission to observe the Sun, that consists on parking two probes, one at L_4 and the other at L_5 practical stability region. To transfer there we propose to use the invariant manifolds related to $L_{1,2}$. The feasibility and cost of such transfer trajectories is going to be studied soon.

ACKNOWLEDGMENT

The research by AF has been supported by the Spanish grant MTM2015-67724-P (MINECO/FEDER) and the Catalan grant 2014 SGR 1145. The research by NM has been supported by the Spanish grant MTM2016-80117-P (MINECO/FEDER) and the Catalan grant 2014 SGR 1145.

The authors would also like to thank J. Timoneda for the maintenance task of the computing facilities of the Dynamical System Group and the Facultat de Matemàtiques i Informàtica of the Universitat de Barcelona, that have largely been used in this work.

REFERENCES

[1] R. Sood and K. Howell, "L_4, L_5 Solar Sail Transfers and Trajectory Design: Solar Observations and Potential Earth Trojan Exploration," *26th AAS/AIAA Space Flight Mechanics Meeting*, February 2016.

[2] A. Farrés, "Transfer orbits to L_4 with a solar sail in the Earth-Sun system," *Acta Astronautica*, Vol. 137, August 2017, pp. 78–90.

[3] A. Farrés and À. Jorba, "Periodic and Quasi-Periodic motions of a Solar Sail around the family SL_1 on the Sun-Earth System," *Celestial Mechanics and Dynamical Astronomy*, Vol. 107, 2010, pp. 233–253.

[4] G. Gómez, À. Jorba, J. Masdemont, and C. Simó, *Dynamics and Mission Design Near Libration Points - Volume IV: Advanced Methods for Triangular Points.*, Vol. 5 of *World Scientific Monograph Series in Mathematics*. World Scientific, 2001.

[5] V. Szebehely, *Theory of orbits. The restricted problem of three bodies*. Academic Press, 1967.

[6] B. Dachwald, W. Seboldt, M. Macdonald, G. Mengali, A. Quarta, C. McInnes, L. Rios-Reyes, D. Scheeres, B. Wie, M. Görlich, *et al.*, "Potential Solar Sail Degradation Effects on Trajectory and Attitude Control," *AAS/AIAA Astrodynamics Specialists Conference*, 2005.

[7] A. McInnes, "Strategies for Solar Sail Mission Design in the Circular Restricted Three-Body Problem," Master's thesis, Purdue University, August 2000.

[8] C. McInnes, *Solar Sailing: Technology, Dynamics and Mission Applications*. Springer-Praxis, 1999.

[9] M. Sevryuki, *Reversible Systems*. Berlin: Springer-Verlag, 1986.

[10] J. Lamb and J. Roberts, "Time-reversal symmetry in dynamical systems: a survey," *Phys. D*, Vol. 112, 1998, pp. 1–39.

[11] A. Farrés and À. Jorba, "On the High Order Approximation of the Centre Manifold for ODEs," *Discrete and Continuous Dynamical Systems - Series B (DCDS-B)*, Vol. 14, October 2010, pp. 977–1000.

[12] C. McInnes, A. McDonald, J. Simmons, and E. MacDonald, "Solar Sail Parking in Restricted Three-Body System," *Journal of Guidance, Control and Dynamics*, Vol. 17, No. 2, 1994, pp. 399–406.

[13] A. Farrés, *Contribution to the Dynamics of a Solar Sail in the Earth-Sun System*. PhD thesis, Universitat de Barcelona, 2009.

[14] A. Giorgilli, A. Delshams, E. Fontich, L. Galgani, and C. Simó, "Effective stability for a Hamiltonian system near an elliptic equilibrium point, with an application to the restricted three-body problem," *J. Differential Equations*, Vol. 77, No. 1, 1989, pp. 167–198, 10.1016/0022-0396(89)90161-7.

[15] C. Simó, "Boundaries of Stability," Slides.

[16] C. Simó, P. Sousa-Silva, and M. Terra, "Practical stability domains near $L_{4,5}$ in the restricted three-body problem: some preliminary facts," *Progress and challenges in dynamical systems*, Vol. 54 of *Springer Proc. Math. Stat.*, pp. 367–382, Springer, Heidelberg, 2013, 10.1007/978-3-642-38830-9_23.